Journal of Solid State Chemistry 181 (2008) 2046–2057

Contents lists available at ScienceDirect

Journal of Solid State Chemistry

journal homepage: www.elsevier.com/locate/jssc

PMo or PW heteropoly acids supported on MCM-41 silica nanoparticles: Characterisation and FT-IR study of the adsorption of 2-butanol

Daniel Carriazo [a], Concepción Domingo [b], Cristina Martín [a], Vicente Rives [a,*]

[a] GIR-QUESCAT, Dpto. de Química Inorgánica, Universidad de Salamanca, 37008-Salamanca, Spain
[b] Instituto de Estructura de la Materia, C.S.I.C., Serrano, 123, 28006-Madrid, Spain

ARTICLE INFO

Article history:
Received 29 January 2008
Received in revised form
29 April 2008
Accepted 4 May 2008
Available online 10 May 2008

Keywords:
Hetero-polyoxometalates
MCM-41
Decomposition of 2-butanol
FT-IR spectroscopy

ABSTRACT

Mesoporous silica, prepared in basic conditions, has been loaded (20% weight) with 12-molybdophosphoric (PMo) or 12-tungstophosphoric (PW) acid and calcined at different temperatures ranging between 250 and 550 °C. The samples have been characterised by N_2 adsorption–desorption at −196 °C, transmission electron microscopy (TEM), powder X-ray diffraction (PXRD), UV–visible diffuse reflectance, Raman spectroscopy and temperature programmed reduction (TPR). The acidity and catalytic activity have been, respectively, examined by monitoring the adsorption of pyridine and 2-butanol by FT-IR spectroscopy. The results indicate that PW and PMo acids are highly dispersed on mesoporous silica MCM-41 spherical nanoparticles. While PMo retains its Keggin structure up to 550 °C, PW decomposes at this temperature into crystalline WO_3 and phosphorous oxides. In both cases, the morphology, hexagonal symmetry and long-range order observed for the support are preserved with calcination up to 450 °C. The Brönsted-type acid sites found in all samples, whose surface concentration decreases as the calcination temperature increases, are responsible for the selective formation of *cis*-butene detected upon adsorption of 2-butanol. The sample containing PW calcined at 450 °C also shows selectivity to methyl ethyl ketone.

1. Introduction

Heteropoly anions such as 12-molybdophosphate or 12-tungstophosphate are polymeric oxoanions formed by condensation of more than two different mononuclear oxoanions, $12WO_4^{2-}+HPO_4^{2-}$ or $12MoO_4^{2-}+HPO_4^{2-}$, respectively. When in the protonated forms, they are known as heteropoly acids (HPAs). Heteropoly anions with the Keggin-type structure show a tetrahedral symmetry based on a central PO_4 unit surrounded by twelve WO_6 or MoO_6 octahedral moieties [1].

The properties of these compounds and their applications in catalysis (both homogeneous and heterogeneous) have been widely studied and reported in the literature in the last decades [2–7]. Their success in the catalysis field is associated to their redox character and strong Brönsted-type acidity, and these properties are easily tuneable by varying their compositions [2,8,9].

Solid HPAs can act as heterogeneous catalysts in liquid phase only in non-polar solvents because they are highly soluble in polar ones. Additionally to the problems associated to the homogeneous catalysis, in terms of recycle and reuse, these compounds exhibit very low-specific surfaces areas (1–10 $m^2 g^{-1}$) [10] and moderate thermal stability, which limit their applications in processes at high temperature. According to different studies reported in the literature, crystalline molybdophosphoric acid (PMo) is decomposed between 375 [2,11] and 400 °C [12], and its Keggin structure is completely destroyed at 450 °C. Regarding the tungtophosphoric acid (PW), decomposition starts at 465 °C [2] and at 610 °C it is completely transformed into P_2O_5 and WO_3 [2,11]. Aiming to overcome these handicaps, HPAs have been supported over different solid matrices. Several conventional supports have been used for dispersing HPAs, namely, silica [13–15], zirconia [14,16], activated carbon [17], etc. However, solids with high specific surface area (around 1000 $m^2 g^{-1}$), narrow pore size distributions, and pore size between 2 and 10 nm, such as mesoporous silica (MCM-41, MCM-48, SBA-15, etc.) [18–19], are excellent support for acid catalysts, allowing a better dispersion of the active phase, even for very large HPA-loading contents. Kozhevnikov et al. [2,20] claimed that the HPA units are highly dispersed on MCM-41 even for loading as high as 50% in weight of polyoxometalate, since they did not detect HPA crystalline phases through X-ray diffraction. The dispersion increases the concentration of active sites and as a consequence their catalytic activity. Mesoporous silica shows other interesting features such as tuneable pore size and particle morphology, which can be tuned by modifying some

* Corresponding author. Fax: +34 923 29 45 74.
E-mail address: vrives@usal.es (V. Rives).

0022-4596/$ - see front matter © 2008 Elsevier Inc. All rights reserved.
doi:10.1016/j.jssc.2008.05.004

synthetic parameters such as surfactant nature and size, stirring rate, dilution, pH, etc., which makes them suitable supports for the immobilisation of these species [21]. The catalytic activity of HPA/MCM-41 systems has been successfully tested in numerous reactions, e.g., alkylation of aromatics [22,23], acetalysation of carbonyl compounds [24,25], carboesterification of carboxylic acids [26,27], D-xylose dehydration [28], etc., showing in most of the cases similar or better performances in terms of activity and selectivity than the unsupported HPA.

The thermal stability of the HPA is a very important factor to be taken into account when using these compounds in a catalytic process, since it can limit the reaction temperature conditions. It is well known that basic solids such as MgO tend to decompose HPAs [2,29]; however, silica, activated carbon or silica-alumina mesoporous solids show optimum surface properties to host these sorts of species. Different results regarding the stability of these species against calcination have been reported for systems prepared upon dispersion of PMo or PW over SiO_2. Kasztelan et al. [30] found that these species do not decompose upon calcination up to 573 °C, while Rocchioccioli-Deltcheff et al. [31] claimed that the HPAs are completely decomposed at 250 °C, a temperature which is lower than that one detected for decomposition of bulk HPA. On the other hand, Yu et al. [32] detected a worsening of the thermal stability of tungstophosphoric species when these are supported on SBA-15; in this case, they reported that HPA decomposes at 410 °C, also a temperature lower than that one detected for decomposition of bulk PW. A similar behaviour was observed by Cheng and Luthra [33] when supporting these heteropoly acids (HPAs) on alumina, whereas Damyanova et al. [9,13] have claimed that the incorporation of PMo on TiO_2 produces an improvement on the polyoxometalate thermal stability, which maintains its Keggin structure at higher temperatures than that measured for the unsupported HPA. These authors also claimed that the insertion or substitution of some cations into the hexagonal mesoporous silicate frameworks, produces structural changes which influence the surface properties of the support, and as a consequence the decomposition of Keggin units of PMo and PW in samples containing Ti or Al is delayed. A partial degradation of the anion was observed in the case of samples doped with zirconium, especially in the case of samples containing molybdophosphate acid [34]. The reviewed literature concludes that the thermal stability of the HPA depends on the nature of the support, HPA-loading amount, and HPA-support interactions.

Due to the significant importance that the thermal stability of HPA supported on different systems, which may limit their activity in catalytic processes, and taking into account that in most of the papers already published about this topic the stability is mainly examined through the relationship with the loaded amounts and not to their evolution with temperature, in this work we have prepared PW and PMo supported over spherical nanoparticles of silica MCM-41 systems, aiming to analyse the possible influence that the particles size and morphology of the matrix may have on the thermal stability of the HPAs studied. These samples have been characterised and their thermal evolution studied in the 250–550 °C range. In addition, the catalytic activities of these samples have been qualitatively evaluated in the decomposition of 2-butanol monitored by FT-IR spectroscopy, a process which has not bee reported previously.

2. Experimental

2.1. Sample preparation

Preparation of the MCM-41 support was carried out following the method described by Cai et al. [35] with some differences: Hexadecyl-trimethylammonium bromide (CTAB) was used as the cationic surfactant, tetraethylorthosilicate (TEOS) was selected as a silica source, and aqueous NaOH as the catalyst solution. The molar ratio chosen was 1(TEOS):0.31(NaOH):0.125 (CTAB):1200(H_2O). An amount of 3.5 mL NaOH 2 M and 1 g CTAB were added to 500 mL H_2O; after dissolution of the surfactant, 5.0 mL of TEOS were slowly added to the solution under continuous stirring at 60 °C. When the addition was completed the mixture was stirred for 0.5 h and then it was submitted to hydrothermal treatment in a stainless-steel vessel for 10 h in an oven at 100 °C. The solid was recovered by filtration, washed with distilled hot water, dried, and calcined in air at 540 °C for 4 h at a heating rate of 1 °C min^{-1}.

The HPA was incorporated by wet impregnation. A portion of 1.0 g of MCM-41 was added to a solution of $H_3PW_{12}O_{40} \times H_2O$ (PW, Fluka), or $H_3PMo_{12}O_{40} \times H_2O$ (PMo, Fluka), prepared by dissolving in 20 mL of distilled water the amount of HPA required for a 20% weight loading. The mixture was stirred for 10 h at 60 °C until the solvent was evaporated; the solid was then dried in a desiccator under vacuum and calcined at different temperatures, from 250 to 550 °C. The solids are denoted as PX1, PX2 and PX3 (X = Mo or W), where numbers are associated to the following temperature treatments: (1) 250 °C, (2) 450 °C, and (3) 550 °C. Once the samples were calcined they were kept in a desiccator under vacuum until used for characterisation or catalysis studies.

2.2. Characterisation techniques

The powder X-ray diffraction (PXRD) patterns were collected on a Siemens D-500 instrument, using Cu $K\alpha$ radiation ($\lambda = 1.54050$ Å) and quartz as an external standard.

Dispersive Raman spectra excited at 514 nm laser wavelength were obtained with a confocal Raman microscope from Renishaw, RM-2000, equipped with a Leica microscope, and an electrically refrigerated CCD camera. The spectra were taken with a 50 × objective (0.75 NA) and 10 mW laser power. Integration times were in the 300–500 s range.

Temperature programmed reduction (TPR) analyses were carried out in a Micromeritics TPR/TPD 2900 instrument at a heating rate of 10 °C min^{-1} and using ca. 30 mg of sample and a H_2/Ar (5% vol., from L'Air Liquide, Spain) mixture as the reducing agent (60 mL min^{-1}).

The Vis–UV spectra were recorded in the 200–1100 nm range in a Perkin-Elmer Lambda 35 apparatus equipped with a Labsphere RSA-PE-20 accessory by the diffuse reflectance technique; MgO was used as a reference.

The textural properties were studied by N_2 adsorption–desorption at −196 °C recorded in a Gemini instrument from Micromeritics. The samples were previously outgassed at 150 °C for 3 h.

Transmission electron microscopy (TEM) pictures were registered in a Zeiss-902 instrument equipped with a digital camera; the samples were prepared on a copper grid by evaporating a drop of water-dispersed sample.

Surface acidity was studied through FT-IR spectroscopic monitoring of pyridine (Py) adsorption in a Perkin-Elmer 16PC spectrometer coupled to a high-vacuum Pyrex system. Self-supported disks were used, outgassed *in situ* in a special cell (built in Pyrex with CaF_2 windows) [36] at 400 °C for 2 h prior to Py adsorption. Twenty scans were taken to improve the signal-to-noise ratio at a nominal resolution of 2 cm^{-1}. The gas was admitted to the IR cell at room temperature. After 15 m of equilibration, the gas phase was removed by outgassing at different temperatures (from room temperature, r.t., to 400 °C) and the spectrum was recorded.

The same special cell was used to study the adsorption of 2-butanol. In this case an amount of 2-butanol vapour (10 mbar) was admitted into the cell where the solid (0.02 g in self-supported disks) had been previously outgassed for 2 h at selected temperatures (250 °C for samples PX1 or 400 °C for samples PX2 and PX3). The FT-IR spectra were collected without previous outgassing the gas phase at different temperatures ranging from r.t. to 250 °C (samples PX1) or 350 °C (samples PX2 and PX3).

3. Results and discussion

3.1. Structural characterisation of the catalysts

3.1.1. PXRD

The diffraction patterns recorded for the support and for samples loaded with HPAs and calcined at different temperatures are shown in Fig. 1. The diffractogram of the support shows four diffraction peaks, the first one, at 39.33 Å ($2\theta = 2.25^\circ$), much more intense than those registered at 22.95 ($2\theta = 3.85^\circ$), 20.08 ($2\theta = 4.40^\circ$) and 15.37 Å ($2\theta = 5.75^\circ$). These maxima are assigned to the diffraction planes (100), (110), (200) and (210), respectively, associated to hexagonal mesoporous silica, MCM-41 [18]. The good resolution of these diffraction peaks suggests a perfect long-range order in this material [37,38]. The diffraction patterns corresponding to all samples, except PMo3, still show the first three peaks assigned to the pristine support, although with lower intensity than for bare MCM-41. This decrease in intensity has been correlated to a loss of structural order or to the scattering contrast between the silicate wall and the sorbate inside the channels [39]. In addition to a strong decrease in the peak intensities, the diffraction patterns of the samples calcined at high temperature (550 °C, samples PX3) show a shift of the (100) peak to higher 2θ values, at 2.44° (36.71 Å) for sample PMo3 and at 2.33° (38.50 Å) for sample PW3. The diffraction pattern corresponding to sample PW3 also shows weak peaks between 20° and 70° assigned to crystalline hexagonal WO_3 (JCPDS file 33–1387) (inset in Fig. 1). Therefore, impregnation of silica with HPA solutions and the thermal treatments given to the samples do not destroy the pristine hexagonal symmetry and only at high temperatures (550 °C) the long-range order of the support decreases noticeably.

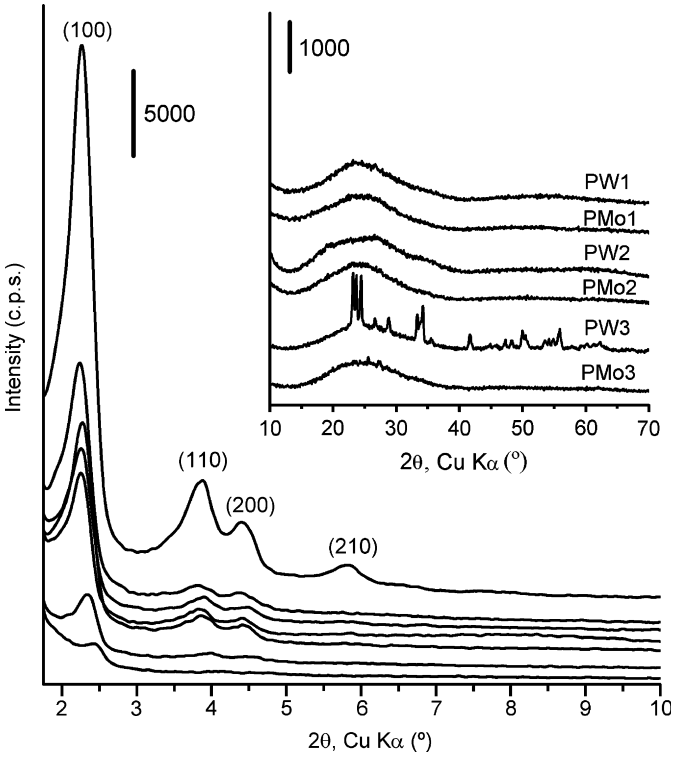

Fig. 1. X-ray diffraction patterns corresponding to different samples, from top: MCM-41, PW1, PMo1, PMo2, PW2, PW3, PMo3; *inset*: diffraction patterns acquired in the 2θ range 10–70 corresponding to labelled samples.

The absence of peaks due to crystalline HPA phases in the diffraction patterns of samples loaded with PMo and PW suggests that the active phase is well dispersed or amorphous, contrary to the behaviour observed in conventional HPA/SiO_2 systems with lower specific surface area and with similar HPA loadings, for which diffraction peaks associated to crystalline HPAs are observed [14].

The regular distance between the centres of two neighbour pores in MCM-41, a_o, can be calculated from the equation $a_o = (2/\sqrt{3})d_{100}$. The values determined for all samples and for the support are summarised in Table 1. The a_o value is 4.54 nm for all samples except for those calcined at 550 °C, for which the value obtained is slightly lower. The pore wall thickness can be estimated by subtracting the value of the pore diameter (as calculated from the nitrogen adsorption–desorption isotherms, see Table 1) from that for the lattice parameter. In this way, a value close to 1.59 nm is obtained for the support and almost all samples. This parameter is a good indicator of the quality (stability) of the mesoporous material; therefore, from these results we can conclude that the MCM-41 silica here synthesised shows a high quality even after HPA anchoring.

3.1.2. Nitrogen adsorption–desorption at −196 °C

The isotherms recorded for all solids prepared are included in Fig. 2. According to the IUPAC classification [40] they correspond to type IV, typical of mesoporous materials. In all of these isotherms up to five regions, characteristic of this sort of isotherms, can be clearly distinguished: (1) monolayer adsorption on the surface, (2) multilayer adsorption, (3) capillary condensation inside mesopores, (4) multilayer adsorption on the external surface and (5) condensation of nitrogen within the interstitial voids between the MCM-41 particles. The capillary condensation of nitrogen inside the mesopores occurs in the p/p° range 0.3–0.4 in all cases.

All pore size distribution curves (Fig. 3) show narrow profiles with a single peak. The maximum of the curve is recorded at 2.9 nm for the support, with an appreciable shoulder that extends up to ca. 3.5 nm. In samples loaded with HPA and subsequently heated at 250 °C, whatever the precise nature of the HPA loaded (PW or PMo), the height of the curve slightly decreases and becomes sharper, probably as a consequence of the blockage of the largest pores (between 3 and 3.5 nm) detected in the bare

Table 1
Lattice and textural properties

Sample	S_{BET} ($m^2 g^{-1}$)	V_P ($mL g^{-1}$)[a]	a_o (nm)[b]	d_p (nm)[c]
MCM-41	1100	0.90	4.54	2.95
PMo1	958	0.68	4.54	2.95
PMo2	740	0.50	4.54	2.95
PMo3	462	0.31	4.23	2.52
PW1	804	0.60	4.54	2.95
PW2	845	0.57	4.54	2.95
PW3	763	0.51	4.42	2.78

[a] Determined at p/p° = 0.95.
[b] Lattice parameter determine by $(2/\sqrt{3})d_{100}$ according to the hexagonal unit cell.
[c] Pore diameter determine by N_2 adsorption.

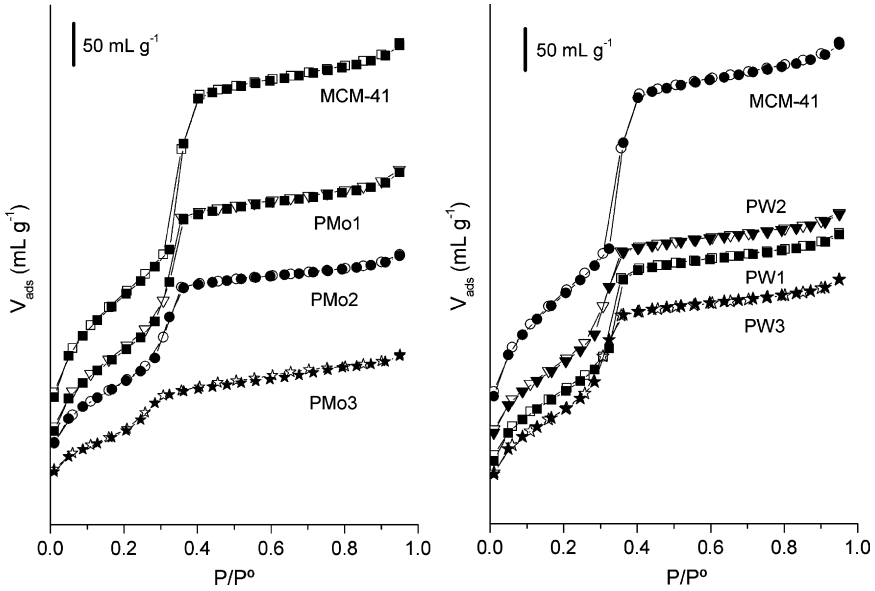

Fig. 2. Nitrogen adsorption (filled symbols)–desorption (open symbols) isotherms register at −196 °C for labelled samples.

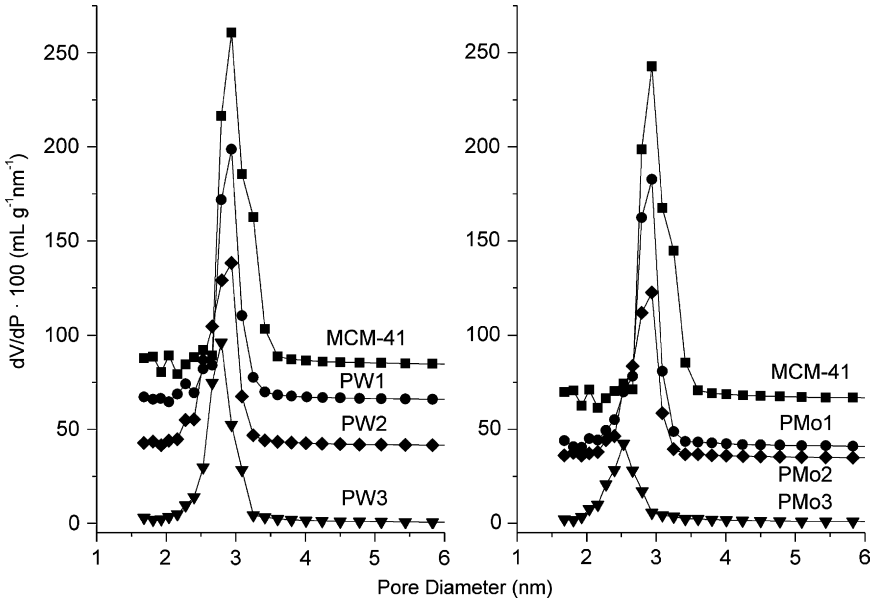

Fig. 3. Pore distribution curves corresponding to labelled samples.

support. When increasing the calcination temperature up to 450 °C the height of the curves further decrease, especially for samples loaded with PMo, for which a low contribution from pores with a smaller diameter (2.5 nm) is detected. The curves corresponding to samples PW3 and PMo3 calcined at 550 °C show a shift in the position of their maxima to 2.80 and 2.32 nm, respectively. The curve for sample PW3 is quite similar to that observed for samples calcined at lower temperatures or for the bare support, while the intensity of the maximum for sample PMo3 strongly decreases.

These changes in the porosity with the HPAs loading produces a progressive decrease in the pore volume as the calcination temperature is increased (Table 1) especially for the PMo-containing samples. Similar changes are observed for the specific surface areas (Table 1). The specific surface area decrease observed for samples PMo as the calcination temperature increases is very noticeable; however, calcination has only a minor effect on the specific surface area of the PW samples: even an increase is observed for sample PW2, calcined at 450 °C. This phenomenon is probably due to the fact that at this temperature the tungtophosphate units undergo a better dispersion. In a general way, we can say that the specific surface areas values for the HPA-loaded solids are higher than those reported by other groups for similar samples with same (or similar) loading, mainly in the case of PW/MCM-41 system [25].

From these results it can be thought that the HPAs units, with a diameter close to 1.2 nm, are preferentially located inside the MCM-41 pores, which do not become completely filled for such loading percentages, rather than on the external surface; calcination at increasing temperatures causes a progressive pore occlusion, especially in sample PMo3.

Taking into account that the average surface occupied per Keggin anion is about 1.44 nm^2, a loading of 20% in weight correspond to areas of 112 and 76 $m^2 g^{-1}$ for PW and PMo samples,

respectively. These values are between 10 and 15 times smaller than the initially available surface area in the bare support, which would be in agreement with the high dispersion detected by from XRD and Raman spectroscopy (see below) results.

3.1.3. Raman spectroscopy

Raman spectra of crystalline HPAs are included in Fig. 4A and B. They show bands at 999, 971, 909, 607 and 250 cm^{-1} for 12-molybdophosphoric acid, and at 1009, 991, 924, 535 and 213 cm^{-1}, in the case of 12-tungstophosphoric acid. The positions of these bands are in agreement with values previously reported in the literature for these compounds. [41] Their ascription to different vibrational modes is summarised in Table 2. After dispersing PMo over MCM-41 and subsequent calcination, whatever the calcination temperature, the same bands previously registered for the pure HPA are observed (although with a poorer resolution), except that one assigned to mode $\nu_{as}(Mo–O_d)$, not observed in the spectrum of sample PMo1 and only weakly detected in those for samples PMo2 and PMo3. A decrease in the intensity and a broadening of the bands as the calcination temperature increases is also observed. It should be noticed that bands characteristic of MoO_3 are not observed, suggesting that the heteropoly anion maintains its Keggin-type structure at least up to 550 °C. The amorphisation observed (broadening of the diffraction maxima) as the calcination temperature increases is probably due to a reinforcement of the interaction of the molybdophosphate with the silanol groups existing on the support pore walls (is an acid–base reaction where the silanol groups act as a base and HPA as a Brönsted acid giving rise to $(SiOH_2^+)(H_2\ PX_{12}O_{40}^-)$ moieties) [42]. On being supported on the mesoporous solid, molybdophosphate is thermally stabilised, as crystalline MoO_3 was not observed in any case, while it was detected when pure HPAs are calcined at 350 °C [2] or 380 °C [12].

Regarding the PW samples (Fig. 4B and Table 2) only the spectrum corresponding to sample PW1 shows the bands assigned to Keggin units. In the spectrum corresponding to the sample calcined at 450 °C, PW2, it is difficult to distinguish even the most intense HPA band around 1000 cm^{-1}, assigned to mode $\nu_s(W–O_d)$, suggesting that the tungstophosphate species are highly dispersed. When the sample is calcined at 550 °C (sample PW3), new very well-defined bands develop at 804, 718, 327 and 270 cm^{-1}, characteristic of crystalline WO_3 [43,44], together with a broad band at about 990 cm^{-1} that has been attributed to well-dispersed polytungstate units [45]; so, some units with the Keggin-like structure seem to remain even after calcination at 550 °C. Crystallisation of WO_3 takes place at higher temperature than for pure 12-tungstophosphoric (465 °C) [2].

The strongest interaction between HPA molecule and the silanol groups, observed for the PW containing sample, is a consequence of the strongest acidity of this HPA, and probably of an enhanced surface basicity of MCM-41, which had been prepared in an alkaline medium.

3.1.4. UV–vis spectroscopy

As expected, parent MCM-41 does not show any absorption in the wavelength region studied. UV–vis spectra corresponding to unsupported PMo and PW (Fig. 5A and B) show a band between 220 and 250 nm and other broad band from 260 to 500 nm

Table 2
Ascription (cm^{-1}) of the Raman bands, corresponding to the heteropolyanions, registered in prepared samples and in commercial HPAs

Sample	$\upsilon_s(M–O_d)$	$\upsilon_{as}(M–O_d)$	$\upsilon_s(M–O_c–M)$	$\upsilon_{as(}M–O_b–M)$	$\upsilon_s(M–O_a)$
PMo	999	971	607	909	250
PW	1009	991	535	924	213
PMo1	999	n.d.	607	900	245
PMo2	999	975	610	900	245
PMo3	999	975	612	900	245
PW1	1009	991	535	925	213
PW2	n.d.	n.d.	n.d.	n.d.	n.d.
PW3[a]	980	n.d.	n.d.	n.d.	n.d.

n.d.: not detected.
[a] Also show bands corresponding to WO_3 at 804 (υ(W–O)), 718, 327 and 270 cm^{-1}.

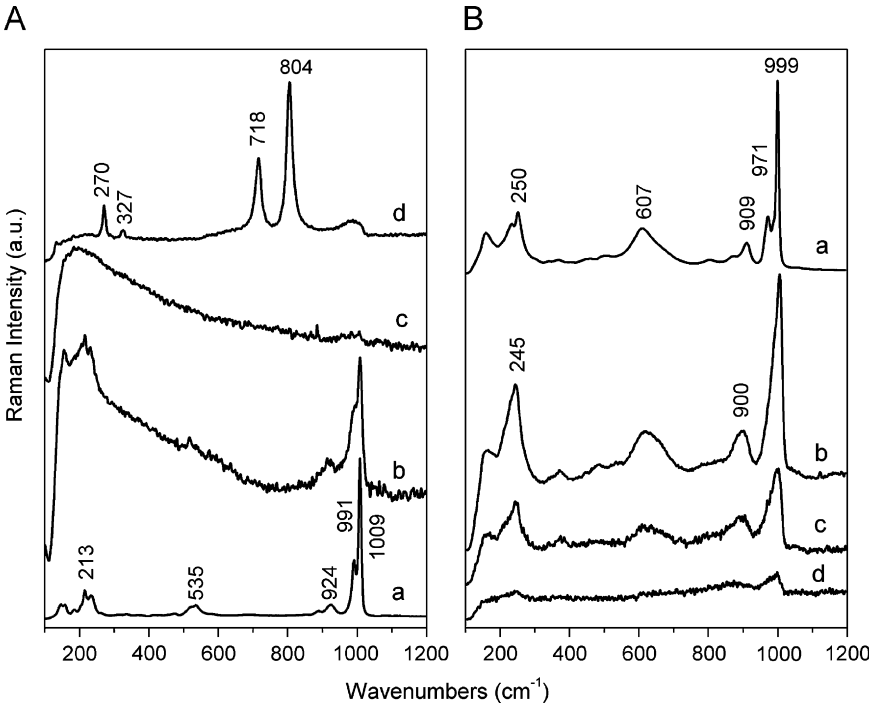

Fig. 4. Raman spectra registered for samples: (A) (a) PW × 1/5, (b) PW1, (c) PW2 and (d) PW3 and (B) (a) PMo × 1/5 (b) PMo1, (c) PMo2 and (d) PMo3.

(phosphomolybdic acid) or 400 nm (tungstophosphoric acid). It should be noticed that the UV–vis spectra corresponding to the PMo supported samples are similar whatever the calcination temperature (250, 450 or 550 °C), showing bands at 220 and 330 nm, i.e., shifted towards lower wavelength than for the pristine acid; polymerised polymolybdates show bands in the 220 and 350 nm spectral region [46] originated by charge transfer processes. In the case of the samples containing tungstophosphate the bands assigned to the charge transfer processes (range 200–400 nm) become broader when the calcination temperature is increased, and a new band arises at 400 nm upon calcination at 550 °C, surely ascribed to WO_3 formation, also identified in this sample by Raman spectroscopy and PXRD.

3.1.5. Acidity

The FT-IR spectrum of MCM-41 shows, after adsorption of pyridine, bands at 1597 (8*a* mode) and 1448 cm^{-1} (19*b* mode) (Fig. 6A and B) in agreement with results previously reported by other authors [47,48]. These bands are assigned to adsorption on weak Lewis-type acid sites or to weakly hydrogen-bonded pyridine. These bands are almost completely vanished after outgassing at 200 °C.

Incorporation of HPA (PMo or PW) on MCM-41 and adsorption of pyridine gives rise to the development of both Brönsted-type and Lewis-type acid sites (Fig. 6). Bands assigned to the pyridinium ions are recorded at 1640 (8*a*) and 1540 (19*b*) cm^{-1} and those associated to pyridine coordinated to Lewis-type acid

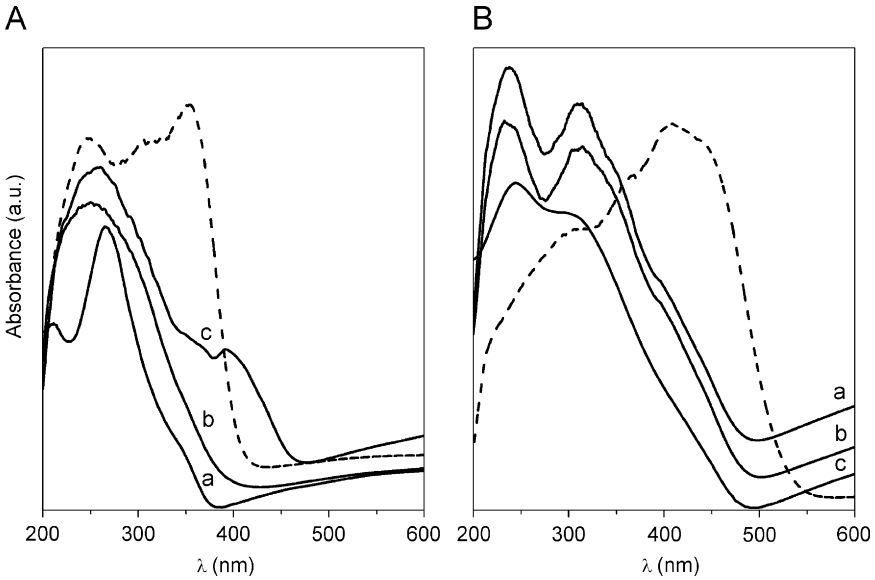

Fig. 5. UV–vis spectra corresponding to samples: (A) (a) PW1, (b) PW2 and (c) PW3 and (B) (a) PMo1, (b) PMo2 and (c) PMo3. Crystalline HPAs PW (A) and PMo (B) are also included (dashed lines).

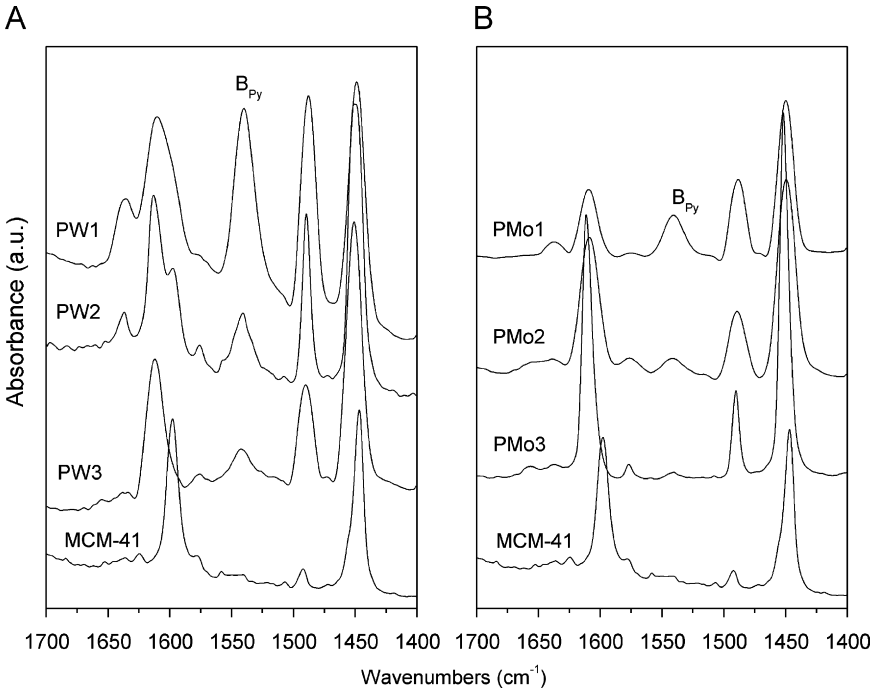

Fig. 6. FT-IR spectra registered over labelled samples after Py adsorption at room temperature (r.t.) and outgassed at 150 °C.

sites at 1610 (8*a*) and 1451 (19*b*) cm^{-1}. When the calcination temperature of the samples is increased (Fig. 6) the intensities of the bands due to the surface Lewis acid sites is hardly modified, even in some cases increases; however, the intensities of the bands due to pyridinium ion decrease, indicating that the Brönsted-type acidity of these samples decreases as the treatment temperature increases. This behaviour can be ascribed, as suggested above, to a decrease in the pore size when the samples are calcined at high temperatures, preventing the access of pyridine to the Brönsted-type acid sites of the heteropoly anion located inside the pores; however, in the case of the samples containing PW it can be also due to decomposition of the Keggin units and formation of the corresponding oxide.

In the case of the PW2 (Fig. 6B) bands assigned to 8*a* and 19*b* modes of coordinated pyridine split into two bands at 1597 and 1612 cm^{-1} and at 1448 and 1451 cm^{-1}, respectively. The positions of the bands registered at low wavenumbers (1597 and 1448 cm^{-1}) are coincident with those recorded after pyridine adsorption on MCM-41, while the other ones are similar to those recorded for all the HPA-containing samples, ascribed to adsorption on Lewis-type acid sites, pointing out that in sample PW2 the weak acid silanol groups are more exposed than in the other samples. This can be tentatively ascribed to the fact that, as the active phase is more dispersed, an easier accessibility of the pyridine molecules to silanol groups which are not interaction with the HPA molecule may occur; actually, this is the only sample which shows an increase in its specific surface area on comparing to the sample calcined at lower temperature.

From these spectra it can be also claimed that samples loaded with PW have a higher concentration of Brönsted-type acid sites than samples loaded with PMo. Both Lewis-type and Brönsted-type acid sites detected in all samples are very strong, since Py remains still adsorbed even after outgassing at 400 °C.

3.1.6. TPR

The reduction curves corresponding to the pure HPAs together with those for the different samples here prepared are included in Fig. 7. As expected, mesoporous silica does not show any reduction peak along the temperature range. Both crystalline HPAs show reduction peaks between 330 and 500 °C that can be ascribed to a loss of reticular oxygen before HPA decomposition takes place [49]. Sharp peaks recorded above 500 °C correspond to the reduction of oxides formed upon thermal decomposition of the HPAs.

In the case of samples loaded with PMo, similar profiles are obtained for samples PMo1 and PMo2, with a maximum reduction rate at 500 °C and broad reduction bands above 600 °C. Sample PMo3 also shows a first peak in approximately the same position, but the second reduction effect is much more intense and well defined at 721 °C. These profiles are similar to that previously observed for polymolybdate species dispersed over different supports such as titania, silica or alumina [50]. The first reduction maximum is assigned to the reduction of the heteropoly anion, which takes place at a higher temperature than for crystalline HPA due to the interaction with the support; the effects recorded at higher temperatures are assigned to reduction of the oxides formed upon decomposition of HPA.

Regarding samples loaded with PW, the reduction profiles for PW1 and PW2 (Fig. 7B) are very similar to each other, with a weak reduction effect at 480 °C and a very intense one at 770 °C, together with a shoulder at 840 °C. The first reduction peak is absent in the profile for sample PW3, and the most intense one splits into three peaks at 755, 781 and 845 °C. These profiles are similar to that previously observed for WO_x/SiO_2 systems, in which formation of tungstosilicic acid was confirmed by EXAFS [51]. As for samples containing PMo, the peak registered at low temperature, 480 °C, can be ascribed to a partial reduction of the W^{6+} within the Keggin unit, while the most intense band, especially that registered for sample PW3, is coincident with the reduction profile associated to crystalline WO_3 (two peaks in the range 730–830 °C).

The H_2 consumption calculated from the areas of the peaks in all the temperature range studied and assuming a complete reduction from Mo(VI) to Mo(0) or from W(VI) to W(0), leads to

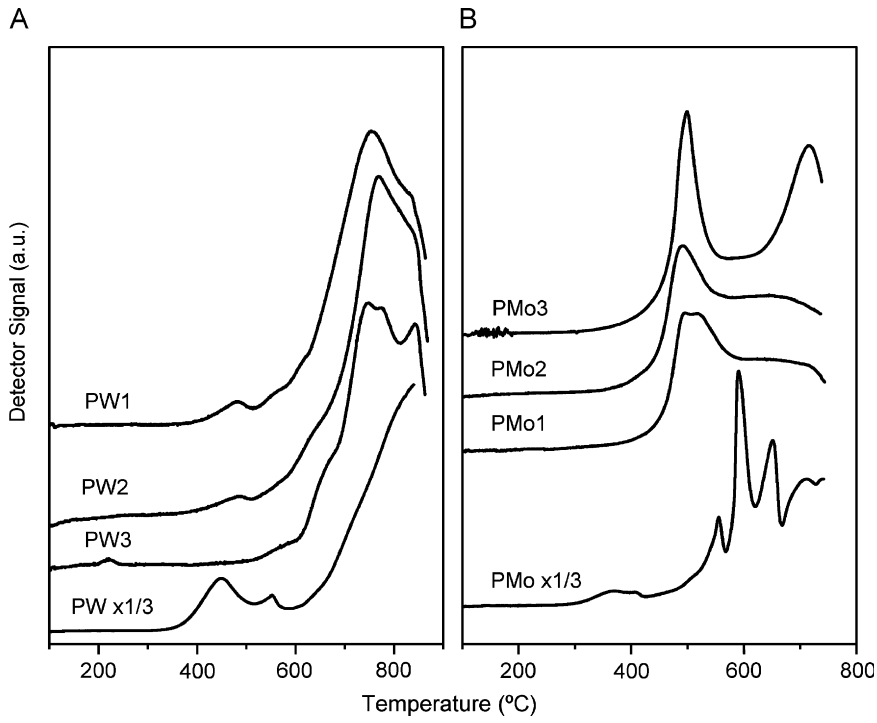

Fig. 7. TPR profiles of the labelled samples.

reduction percentages ranging between 70% and 80%; the largest reducibility is detected in the sample PW2.

3.1.7. TEM

The morphologies and microstructure of the solids here synthesised are revealed by TEM (Fig. 8). Particles consisting of nanospheres or elongated nanospheres with diameters in the range 120 and 200 nm are observed. A narrow pore distribution can be also concluded from the micrographs, in agreement with results above obtained from other techniques.

Incorporation of HPA and calcination at different temperature do not give rise to important changes in the images, which support that HPAs units are very highly dispersed inside the pores; only for samples calcined at 550 °C, the well pore distribution is partially lost, although the particles still retain their pristine morphology.

3.2. FT-IR study of the adsorption of 2-butanol

In order to analyse the influence that structural transformations derived upon calcination within the HPA/MCM-41 systems might have on the catalytic activity, a study of 2-butanol decomposition over the samples prepared has been carried out. This study has been carried out in the absence of oxygen and without removing the vapour phase after adsorption.

The FT-IR spectrum recorded for outgassed MCM-41 (Fig. 9a) show bands at 3740 and 3550 (shoulder) cm^{-1} corresponding to the ν(OH) vibration mode of the silanol groups (SiOH) inside the channels without and with strong hydrogen-bonding interaction, respectively [47,48]. The intense and broad band below 1350 cm^{-1} is assigned to Si–O stretching modes.

Upon 2-butanol adsorption at room temperature (Fig. 9b) a decrease in the intensity of the band corresponding to the ν(OH)

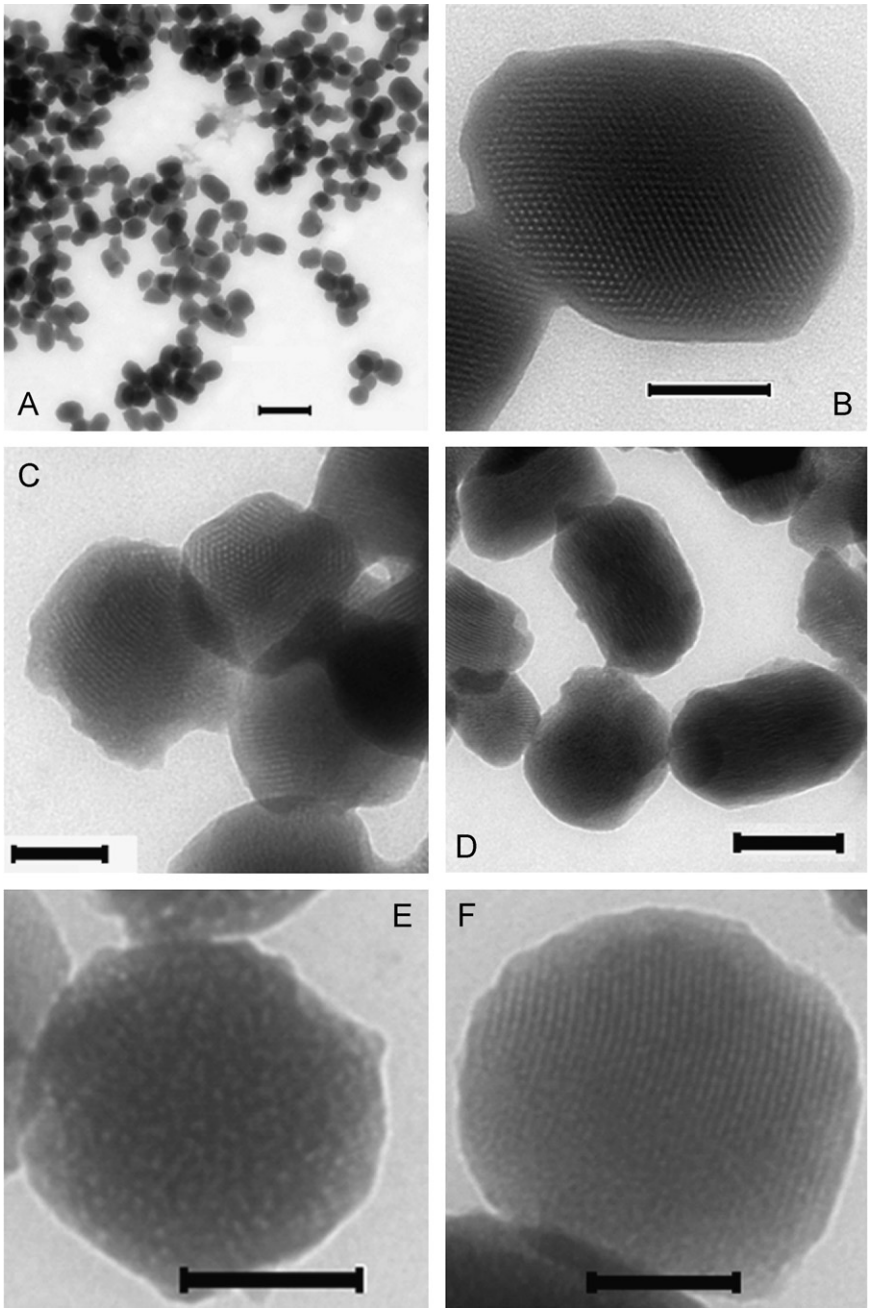

Fig. 8. TEM pictures corresponding to: MCM-41 (a, b), PW2 (c), PMo2 (d), PW3 (e) and PMo3 (f); scale bars: (a) 300 nm, (b) 50 nm and (c–f) 75 nm.

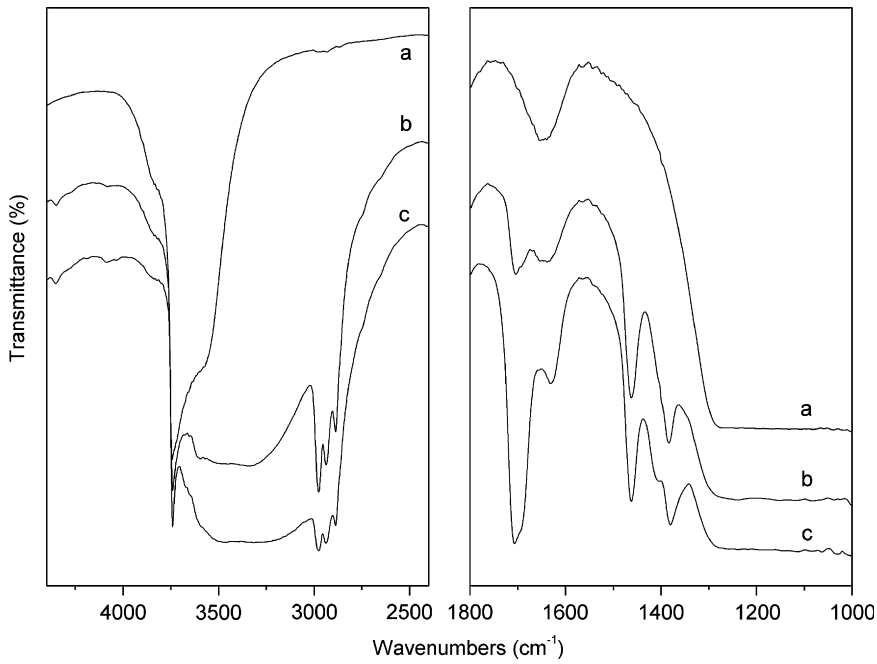

Fig. 9. FT-IR spectra of support MCM-41 (a) outgassed at 400 °C, (b) after 2-butanol adsorption at r.t. and (c) heated at 200 °C.

mode of isolated silanols (3740 cm^{-1}) is observed, together with development of a broad band between 3100 and 3650 cm^{-1}, which is assigned to coordinated molecular 2-butanol or hydrogen-bonded to the surface. Bands at 2975, 2930 and 2885 cm^{-1} corresponding to the ν(C–H) stretching modes of sec-butoxy species can be identified in the high wavenumbers region. The bands corresponding to δ(CH) modes of these species are recorded at 1459 and 1376 cm^{-1}. The broad band that silica shows below 1350 cm^{-1} does not allow to observe other bands characteristic of alkoxides. A medium intensity band at 1702 cm^{-1} corresponding to the ν(C=O) mode of methyl ethyl ketone is also observed upon 2-butanol adsorption at room temperature. Formation of the carbonyl species at a rather low temperature evidences the surface basicity of this support. Previous studies [52] on the adsorption of 2-butanol on silica have demonstrated that the carbonyl is only formed above 100 °C.

Upon heating above 100 °C (Fig. 9c) a general decrease in the intensities of the bands associated to sec-butoxy species, and a simultaneous increase in the intensity of the band assigned to butanone (formed through alcohol dehydrogenation) is observed.

Samples loaded with HPAs and degassed at 250 (samples PX1) or 400 °C (samples PX2 and PX3) show FT-IR spectra similar to that above described for the bare support (Figs. 10–12). No band characteristics of HPAs species are recorded, probably due to its well dispersion over the MCM-41 surface. It should be highlighted that only the spectrum of sample PW2 shows clearly the band corresponding to the ν(OH) mode of isolated silanols at 3740 cm^{-1}, in agreement with the surface acidity results.

The infra-red spectra recorded after 2-butanol adsorption at room temperature are similar to that registered for MCM-41. Some representative sets of spectra are plotted in Figs. 10–12. The band assigned to isolated silanols (SiOH) has vanished in all of them and a broad band between 3650 and 3100 cm^{-1} develops. This band is due to coordinated molecular 2-butanol or hydrogen bonded to the surface, while other bands are ascribed to formation of sec-butoxide species, i.e., those bands at 2974, 2925, 2876 cm^{-1} (ν(CH)), 1462 and 1378 cm^{-1} (δ(CH)). A weak band at 1694 cm^{-1} ascribed to the ν(C=O) mode of butanone can be also distinguished for sample PW2 (Fig. 12).

When the temperature is raised to 200 °C, a decrease in the intensity of the bands assigned to sec-butoxy species is observed and two new bands develop at 3030 and 1620 cm^{-1}. These bands can be assigned to ν(CH=) and ν(CH=CH) modes of *cis*-butene species, since in the gas phase this compound show bands at 1660 and 3030 cm^{-1} [53]. Shifts toward lower wavenumbers are typical of alkene species interacting with surface electron-withdrawing centres through the C=C double bond flat on the surface via the π-orbital. The high preference of the *cis*-product on dehydrogenation of 2-butanol has been explained by Pines and Haag [54]. The presence of but-1-ene can be discarded, as bands at 1856–1800 and 3097–3075 cm^{-1} due to the overtone of the out-of-plane $\delta(CH_2)$ mode and the ν(CH) mode of the vinyl group are not recorded.

In addition to development of bands characteristic of *cis*-butene, an increasing in the intensity of the weak band registered at 1696 cm^{-1} corresponding to the ν(C=O) mode of butanone is also observed for sample PW2 (Fig. 12). The band due to butanone is recorded also, but only as a weak shoulder, in the spectrum for sample PW1.

When heating at 300 °C a slightly increase in the intensity of those bands assigned to the alkene and carbonyl species is observed.

Therefore, adsorption of 2-butanol over PW3, PMo1, PMo2 and PMo3 samples produces *cis*-butene as a single product, while over sample PW2 both *cis*-butene and butanone are produced (small amounts of butanone are also formed on sample PW1). It should be noticed that bands due to carboxylate species have not been detected along all the temperature range (up to 300 °C) studied.

The interaction between the products formed through alcohol decomposition (butanone and/or alkene) with the catalyst surface is rather weak, since these products are desorbed at low outgassing temperatures (around 200 °C).

Despite studies carried out by FT-IR monitoring of adsorption of probe molecules are usually considered qualitative, in this case, and by using similar self-supported wafers (0.02 g) and the same amount of 2-butanol in the vapour phase (10 mbar), some quantitative conclusions can be reached. From the intensity of the band registered at 1620 cm^{-1} corresponding to the ν(CH=CH)

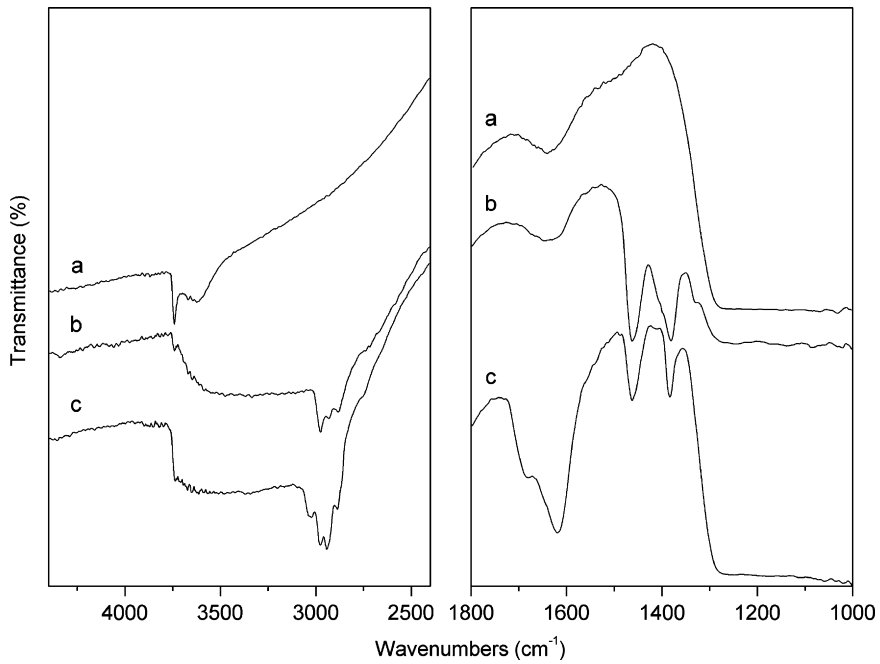

Fig. 10. FT-IR spectra of sample PW1 (a) outgassed at 250 °C, (b) after 2-butanol adsorption at r.t. and (c) heated at 200 °C.

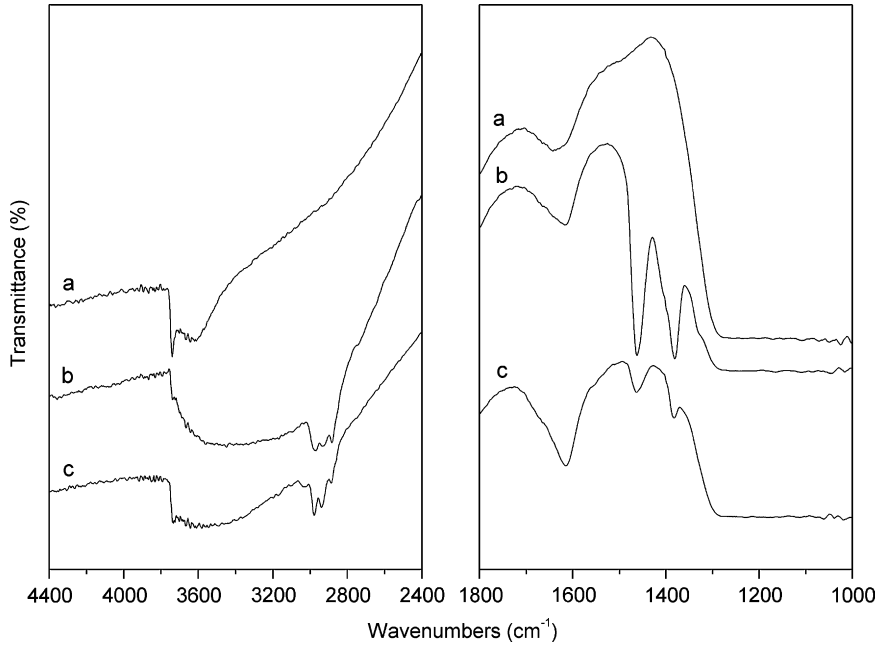

Fig. 11. FT-IR spectra corresponding to sample PMo2 (a) evacuated at 400 °C, (b) after 2-butanol adsorption at r.t. and (c) heated at 200°C.

mode of alkene in the spectra of different samples, we can conclude that samples calcined at 450 °C (PMo2 and PW2) have higher selectivity to *cis*-butene formation, especially PW2 sample. This sample is also selective to butanone formation. In a general way, samples loaded with PW seem more selective toward *cis*-butene formation than ones containing PMo. This behaviour is in agreement with the acidity results obtained in this work, since Brönsted-type acid sites concentration, which are responsible for alcohol dehydration (through a E1 mechanism) [55–57] is larger in samples loaded with PW than in those containing PMo.

It is obvious that the butanone formation through alcohol dehydrogenation over MCM-41 is not an oxidative dehydrogenation process, since there are no redox centres on the surface of this sample. So, it should be formed through a simple dehydrogenation produced by the basic centres (OH^- or O^{2-} species) existing in this solid. However, carbonyl formation over sample PW2 could follow two different ways: (1) simple dehydrogenation, or (2) oxidative dehydrogenation through a Mars and Van Krevelen mechanism [58,59], because in this solid exist centres of different nature, i.e., acid, base and redox (W^{6+}). In order to assess the precise role played by these sites, the following experiment was performed: after being exposed to 2-butanol and calcined at 300 °C, sample PW2 was outgassed at 400 °C for 2 h; in this way all the adsorbed species were desorbed. The spectrum recorded is included in

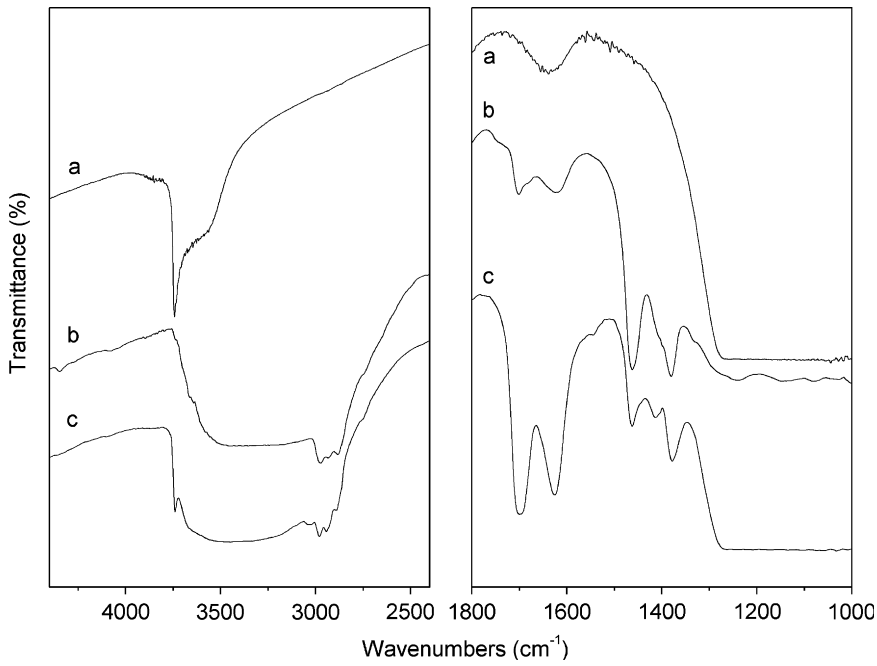

Fig. 12. FT-IR spectra of sample PW2 (a) evacuated at 400 °C, (b) after 2-butanol adsorption at r.t. and (c) heated at 200 °C.

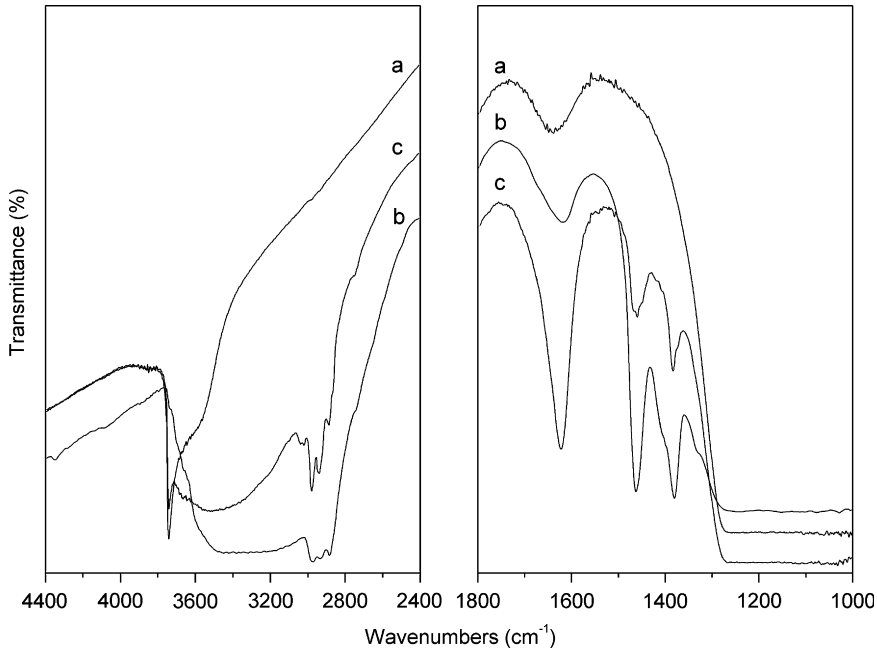

Fig. 13. FT-IR spectra of sample PW2 evacuated at 400 °C, treated with 2-butanol and heated at 300 °C, without remove it from the cell, and outgassed at 400 °C (a) and after 2-butanol adsorption at r.t. (b) and heated at 200 °C (c).

Fig. 13; its profile is similar to that recorded for clean sample (Fig. 12a). After this treatment 2-butanol was again admitted into the cell at room temperature and the sample heated between 100 and 300 °C. The spectra obtained after this second adsorption are plotted also in Fig. 13. As it can be seen, these spectra are different to that registered after the first 2-butanol adsorption. The spectrum recorded after the second does not show bands assigned to butanone whatever the temperature tested, but only those bands associated to *cis*-butene are registered.

When the same experiment was performed with the bare MCM-41 support almost coincident spectra were recorded after the first and the second adsorption steps, with bands due to methyl ethyl ketone. We have also checked that surface acidity is maintained after the first adsorption of butanol on sample PW2, with essentially the same spectrum after adsorption of pyridine.

These studies suggest that the first adsorption of the alcohol over sample PW2 modify the surface sites responsible for carbonyl formation (redox sites/basic sites). The redox surface centres, W^{6+}, only can be deactivated if they have been previously involved in oxidation of the alcohol to methyl ethyl ketone; in other words, if the carbonyl has been produced through oxidative dehydrogenation. As after the first 2-butanol adsorption and subsequent outgassing the sample has not been re-oxidised under air or oxygen, in the second adsorption step the catalyst has not enough

concentration of surface redox centres, and for this reason in this latter case only dehydration to *cis*-butene, catalysed by strong Brönsted-type (H^+) and Lewis-type acid sites, takes place.

4. Conclusions

The results obtained in this study showed that the dispersion of PMo and PW HPAs on the surface of spherical nanoparticles of silica MCM-41 produces an improvement in the thermal stability of the corresponding HPAs. This improvement is especially significant in the case of PMo, preserving its Keggin structure upon calcination up to 550 °C. Calcination at this temperature (550 °C) of samples containing PW gives rise to its decomposition into WO_3 and P_2O_5, probably due to the higher host–guest interactions of this HPA.

In both cases, incorporation of HPA produces a decrease in the specific surface areas, pore size and pore volumes, without modifying the initial isotherms shape which are associated to mesoporous materials in all cases. These results suggest that the HPA units are located inside the pores interacting with the silanol groups of the pores wall, an assumption also supported by the FT-IR results, which showed that in all cases the intensity of the bands assigned to υ(OH) of silanol groups decreases after incorporation of the HPA.

Decomposition of 2-butanol on all this samples gives rise to production of *cis*-butene via dehydration, due to the presence of Brönsted-type acid sites. In the case of samples loaded with PW (mainly PW1 and PW2), a higher selectivity to this product is observed in comparison to that for samples containing PMo, surely due to their higher Brönsted-type acidity.

Moreover, the sample loaded with PW and calcined at 450 °C (PW2) shows an unusual behaviour since, in addition to the formation of *cis*-butene, formation of butanone by oxidative dehydrogenation is also observed on this sample, surely due to its special properties, such as high reducibility of W(VI), high dispersion of the active phases, large specific surface area, and two Lewis-type acid sites (strong ones, W^{6+} ions, and very weak ones, silanol groups of the support) exhibited by this sample.

Acknowledgments

Financial support from MEC (MAT2006-10800-C02-01) and ERDF are acknowledged, D.C. also thanks a grant from Universidad de Salamanca.

References

[1] M.T. Pope, Heteropoly and Isopoly Oxometalates, Springer, Berlin, 1983.
[2] I.V. Kozhevnikov, Chem. Rev. 98 (1998) 171.
[3] N. Mizuno, M. Misono, Chem. Rev. 98 (1998) 199.
[4] Y. Izumi, R. Hasebe, K. Urabe, J. Catal. 84 (1983) 402.
[5] T. Blasco, A. Corma, A. Martinez, P.J. Martinez-Escolano, J. Catal. 177 (1998) 306.
[6] J.H. Kyle, J. Chem. Soc. Dalton Trans. (1983) 2609.
[7] A.S. Dias, M. Pillinger, A.A. Valente, Appl. Catal. A: Gen. 285 (2005) 126.
[8] T. Okuhara, H. Watanabe, T. Nishimura, K. Inumaru, M. Misono, Chem. Mater. 12 (2000) 2230.
[9] S. Damyanova, J.L.G. Fierro, Chem. Mater. 10 (1998) 871.
[10] I.V. Kozhevnikov, Catal. Rev. Sci. Eng. 37 (1995) 311.
[11] I.V. Kozhevnikov, J. Mol. Catal. A: Chem. 262 (2007) 86.
[12] C. Rocchioccioli-Deltcheff, A. Aouissi, M. Bettahar, S. Launay, M. Fournier, J. Catal. 164 (1996) 16.
[13] S. Damyanova, M.L. Cubeiro, J.L.G. Fierro, J. Mol. Catal. A: Chem. 142 (1999) 85.
[14] E. López-Salinas, J.G. Hernández-Cortéz, I. Schifter, E. Torres-García, J. Navarrete, A. Gutiérrez-Carrillo, T. López, P.P. Lottici, D. Bersani, Appl. Catal. A: Gen. 193 (2000) 215.
[15] A. Rives, E. Payen, R. Hubaut, P. Vazquez, L. Picio, C. Cáceres, M. Blanco, Catal. Lett. 71 (2001) 193.
[16] A. De Angelis, S. Amarilli, D. Berti, L. Montanari, C. Perego, J. Mol. Catal. A: Chem. 146 (1999) 37.
[17] Y. Izumi, K. Urabe, Chem. Lett. (1981) 663.
[18] J.S. Beck, J.C. Vartuli, W.J. Roth, M.E. Leonowicz, C.T. Kresge, K.D. Schmitt, C.T.W. Chu, D.H. Olson, E.W. Sheppared, S.B. McCullen, J.B. Higgins, J.L. Schlenker, J. Am. Chem. Soc. 114 (1992) 10834.
[19] A. Corma, Chem. Rev. 97 (1997) 2373.
[20] I.V. Kozhevnikov, A. Sinnema, R.J.J. Jansen, K. Pamin, H. van Bekkum, Catal. Lett. 30 (1995) 241.
[21] Q. Huo, D.I. Margolese, G.D. Stucky, Chem. Mater. 8 (1996) 1147.
[22] X.S. Zhao, G.Q. Lu, C. Song, Chem. Commun. (2001) 2306.
[23] G.D. Yadar, A.D. Murkute, Adv. Synth. Catal. 346 (2004) 389.
[24] K. Shimizu, E. Hayashi, T. Hatamachi, T. Kodama, T. Higuchi, A. Satsuma, Y. Kitayama, J. Catal. 231 (2005) 131.
[25] B. Rabindran Jermy, A. Pandurangan, Appl. Catal. A: Gen. 295 (2005) 185.
[26] K. Nakajima, I. Tomita, M. Hara, S. Hayashi, K. Domen, J.N. Kondo, Adv. Mater. 17 (2005) 1839.
[27] I. Diaz, C. Márquez-Alvarez, F. Mohino, J. Perez-Pariente, E. Sastre, J. Catal. 193 (2000) 295.
[28] A.S. Dias, M. Pillinger, A.A. Valente, Microporous Mesoporous Mater. 94 (2006) 214.
[29] M. Misono, Catal. Rev. Sci. Eng. 30 (1988) 339.
[30] S. Kasztelan, E. Payen, J.B. Moffat, J. Catal. 112 (1988) 320.
[31] C. Rocchioccioli-Deltcheff, M. Amirouche, G. Harve, M. Fournier, M. Che, J.M. Tatibouet, J. Catal. 126 (1990) 591.
[32] S.Y. Yu, L.P. Wang, B. Chen, Y.Y. Gu, J. Li, H.M. Ding, Y.K. Shan, Chem. Eur. J. 11 (2005) 3894.
[33] M.C. Cheng, P. Luthra, J. Catal. 109 (1988) 163.
[34] S. Damyanova, L. Dimitrov, R. Mariscal, J.L.G. Fierro, L. Petrov, I. Sobrados, Appl. Catal. A: Gen. 256 (2003) 183.
[35] Q. Cai, Z.S. Luo, W.Q. Pang, Y.W. Fan, X.H. Chen, F.Z. Cui, Chem. Mater. 13 (2001) 258.
[36] V. Rives, C. Martín, A. Montero, Spanish Patent, 200100688, 2001.
[37] U. Ciesla, F. Schüth, Microporous Mesoporous Mater. 27 (1999) 131.
[38] T.P. Taner, T.J. Pinnavaia, Science 267 (1995) 211.
[39] B. Marler, U. Oberhagemann, S. Vortmann, H. Gies, Microporous Mater. 6 (1996) 375.
[40] K.S.W. Sing, D.H. Everett, R.A.W. Haul, L. Moscou, R. Pierotti, J. Rouquerol, T. Sieminiewska, Pure Appl. Chem. 57 (1985) 603.
[41] R. Thouvenot, M. Fournier, R. Franck, C. Rocchiccioli-Deltcheff, Inorg. Chem. 23 (1984) 598.
[42] F. Lefebvre, J. Chem. Soc. Chem. Commun. (1992) 756.
[43] E. Salje, Acta Crystallogr. A 31 (1975) 360.
[44] E. Haro-Poniatowski, M. Jouanne, J.F. Morhange, C. Julien, R. Diamant, M. Fernández-Guasti, G.A. Fuentes, J.C. Alonso, Appl. Surf. Sci. 127–129 (1998) 674.
[45] E. Payen, S. Kasztelan, Trends Phys. Chem. 4 (1994) 363.
[46] R.S. Weber, J. Catal. 151 (1995) 470.
[47] J. Ward, J. Catal. 9 (1967) 225.
[48] A. Jentys, K. Kleestofer, H. Vinek, Microporous Mesoporous Mater. 27 (1999) 321.
[49] B.K. Hodnett, J.B. Moffat, J. Catal. 91 (1985) 93.
[50] M. del Arco, S.R.G. Carrazan, C. Martín, I. Martín, V. Rives, P. Malet, J. Mater. Chem. 3 (1993) 1313.
[51] C. Martin, P. Malet, G. Solana, V. Rives, J. Phys. Chem. B 102 (1998) 2759.
[52] S.R.G. Carrazán, C. Martín, G. Solana, V. Rives, Langmuir 17 (2001) 6968.
[53] L.J. Bellamy, The Infrared Spectra of Complex Molecules, Chapman & Hall, London, 1975.
[54] H. Pines, W.O. Haag, J. Am. Chem. Soc. 83 (1961) 2847.
[55] F. Figueras Roca, L. De Mourgues, Y. Tranbouze, J. Catal. 14 (1969) 107.
[56] H. Knözinger, A. Scheglila, J. Catal. 17 (1970) 252.
[57] H. Knözinger, R. Kohne, J. Catal. 5 (1966) 264.
[58] P. Mars, D.W. Van Krevelen, Chem. Eng. Sci. 3 (1954) 41.
[59] C. Doornkamp, V. Ponec, J. Mol. Catal. A: Chem. 162 (2000) 19.